Computational investigation of binding mechanism of substituted pyrazinones targeting corticotropin releasing factor-1 receptor deliberated for anti-depressant drug design

Shashank Shekhar Mishra[1], T. Venkatachalam[2], Chandra Shekhar Sharma[3], Hemendra Pratap Singh[3], Sourav Kalra[4], Neeraj Kumar[1*]

[1]Department of Pharmaceutical Chemistry, Geetanjali University, Udaipur-313001, India

[2]Department of Pharmaceutical Chemistry, Annai JKK Sampoorani ammal College of Pharmacy, Namakkal, Tamil Nadu-638183

[3]Department of Pharmaceutical Chemistry, Bhupal Nobles' College of Pharmacy, Bhupal Nobles' University, Udaipur-313001, India

[4]Centre for Human Genetics & Molecular Medicine, Central University of Punjab, Bhatinda-151001, India

E-mail addresses:

shashankmedchem09@gmail.com (Shashank Shekhar Mishra)

venkatachalammpharm@yahoo.co.in (Dr. T. Venkatachalam)

cssharma_medicinalchemistry@yahoo.com (Dr. Chandra Shekhar Sharma)

hps_medicinalchemistry@yahooco.in (Dr. Hemendra Pratap Singh)

nonakalra@gmail.com (Dr. Sourav Kalra)

neerajkumarkamra@gmail.com (Dr. Neeraj Kumar)

*Corresponding author:
Dr. Neeraj Kumar,
Department of Pharmaceutical Chemistry,
Geetanjali Institute of Pharmacy,
Geetanjali University,
Udaipur, Rajasthan, India-313001
E-mail: neerajkumarkamra@gmail.com
Tel.: +919983499298

Graphical Abstract:

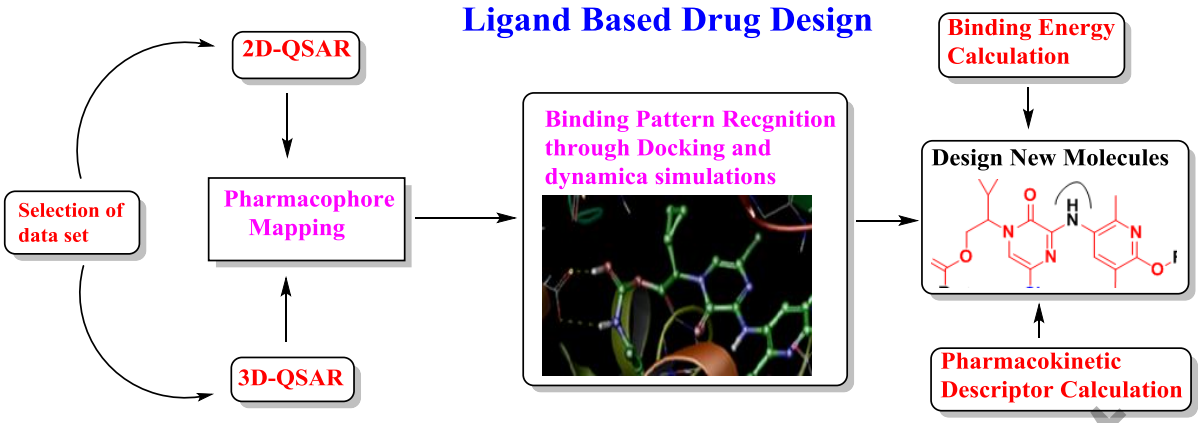

ABSTRACT

In spite of various research investigations towards anti-depressant drug discovery programme, no one drug has not yet launched last 20 years. Corticotropin-releasing factor-1 (CRF-1) is one of the most validated targets for the development of antagonists against depression, anxiety and post traumatic stress disorders. Various research studies suggest that pyrazinone based CRF-1 receptor antagonists were found to be highly potent and efficacious. In this research investigation, we identified the pharmacophore and binding pattern through 2D and 3D-QSAR and molecular docking respectively. Molecular dynamics studies were also performed to explore the binding pattern recognition. We establish the relationship between activity and pharmacophoric features to design new potent compounds. The best 2D-QSAR model was generated through multiple linear regression method with r^2 value of 0.97 and q^2 value of 0.89. Also 3D-QSAR model was obtained through k-nearest neighbor molecular field analysis method with q^2 value of 0.52 and q^2_se value of 0.36. Molecular docking and binding energy were also evaluated to define binding patterns and pharmacophoric groups, including (i) hydrogen bond with residue Asp284, Glu305 and (ii) π-π stacking with residue Trp9. Compound **11i** has the highest binding affinity compared to reference compounds, so this compound could be a potent drug for stress related disorders. Most of the compounds, including reference compounds were found within acceptable range of physicochemical parameters. These observations could be provided the leads for the design and optimization of novel CRF-1 receptor antagonists.

Keywords: CRF-1, Molecular docking, Prime MM/GBSA, Molecular dynamics, QSAR.

List of abbreviations

CRF	Corticotropin-Releasing Factor
HPA	Hypothalamus-Pituitary-Adrenocortical Axis
kNN MFA	k-Nearest Neighbor Molecular Field Analysis
MD	Molecular Dynamics
MLR	Multiple Linear Regression
MM/GBSA	Molecular Mechanics/Generalized Born Surface Area
OLS	Ordinary Least Squares Regression
OPLS	Optimized Potential for Liquid Simulations
POPC	1-palmitoyl-2-oleoyl-sn-glycero-3-phosphocholine
QSAR	Quantitative structure-activity relationship
RMSD	Root Mean Square Deviation
RMSF	Root Mean Square Fluctuation
SA	Simulated Annealing
XP	Extra precision

1. Introduction

Corticotropin-releasing factor (CRF) is made up of 41- amino acid which is the main modulator of hypothalamus-pituitary adrenocortical axis and mediates the endocrine (Williams, 2013), autonomic and behavioural responses to stress (Dzierba et al., 2008; Owens et al., 1991). Two G-protein coupled receptor subtypes of CRF receptor have been identified as CRF-1 and CRF-2 and CRF-1 receptor is mainly distributed throughout the central and peripheral nervous system (Williams, 2013; Kumar et al., 2017). Various research investigations suggest that stress vulnerability increases the CRF secretion in hypothalamus that stimulates the secretion of cortisol (Grigoriadis et al., 2001). Cortisol regulates the secretion of CRF, this process like a negative feedback system works against the activation of the HPA axis (Hauger et al., 2009). However, activation of CRF-1 receptor subtypes results failure of the negative feedback system in stress related disorders and it has been proved that the level of stress responses and anxiety like symptoms was found very less in mice with lack of CRF-1 receptors (Gilligan et al., 2009; Zorrilla and Koob, 2004). These studies revealed that stress related disorders may be treated by blockade of CRF-1 receptors. There are various small molecule CRF-1 receptor antagonists have been reported in the literature, but no one has launched as drug since last 20 years (Mochizuki et al., 2016). The structures of various reported CRF-1 antagonists were depicted in Figure 1. Hence, it is essential to develop reliable and potent drug that can combat stress related disorders by blocking the CRF-1 receptor.

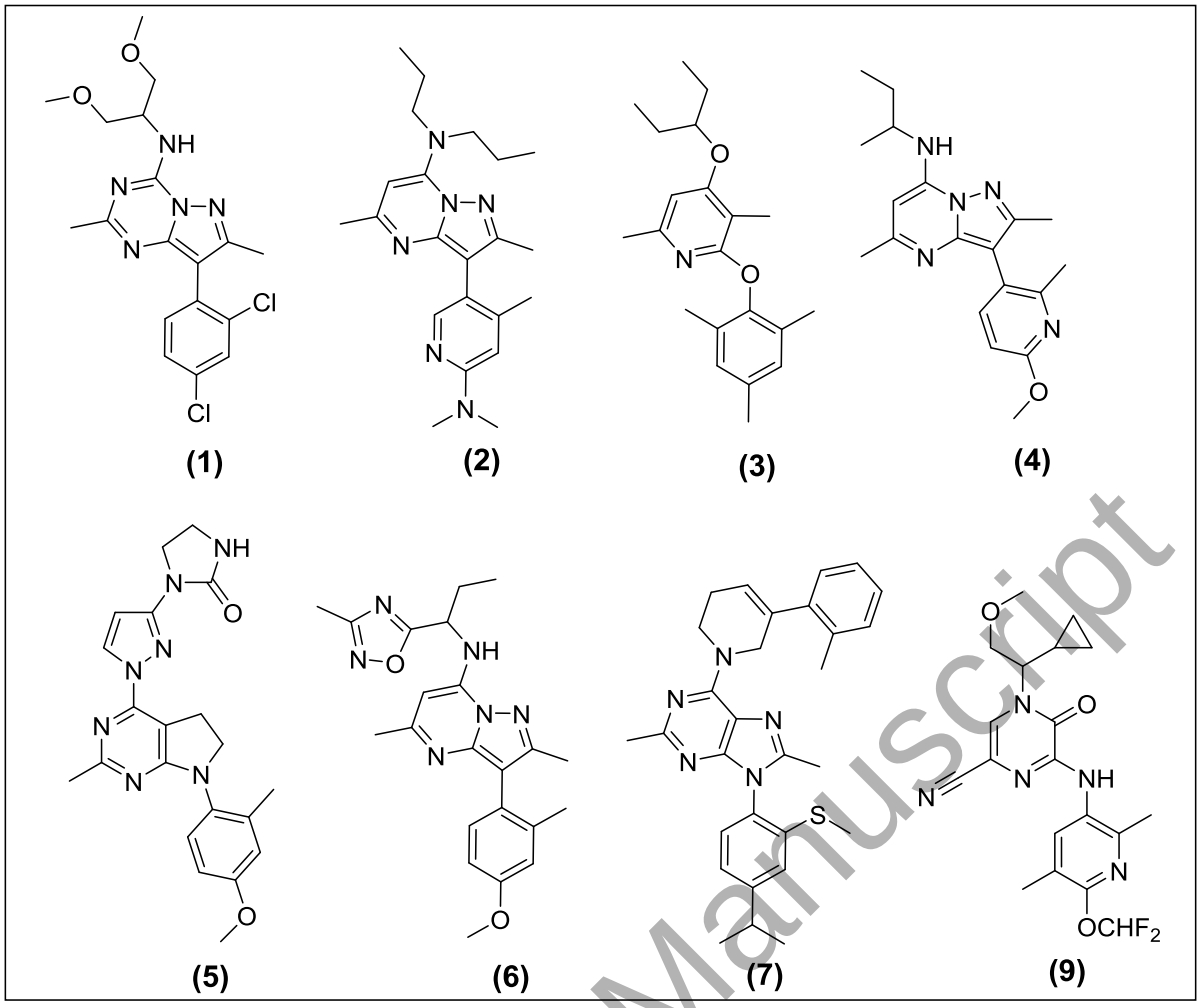

Figure 1: Structure of various reported CRF-1 receptor antagonists (1) DMP696 (2) R121919 (3) CP-316,311 (4) Pexacerfont (5) Emicerfont (6) Oxadiazole derivative (7) Phenyl-substituted 1,2,3,6-tetrahydropyridine (9) BMS-764459

Ligand based drug design is very convenient approach to accelerate the development of medicinally active compounds by studying the large number of molecules that interact with the biological target of interest (Guner et al., 2004). QSAR and pharmacophore mapping is the most popular method for ligand based drug design. QSAR is a computational method to quantify the correlation between the chemical structures of a series of compounds and a particular chemical or biological process. A quantitative relationship is established between the physico-chemical parameters of the active molecules and the biological activity. The developed QSAR model is then utilized to optimize the active compounds to maximize the relevant biological activity. The predicted compounds are then tested experimentally for the desired activity (Acharya et al., 2011). Previously reported studies indicate that pyrazinone based CRF-1 receptor antagonists have been shown excellent selectivity and exquisite

potency (Hartz et al., 2009; Hartz et al., 2009; Hartz et al., 2009; Kaur et al., 2012). An understanding of better binding pattern and SAR analysis would help to resolve the issues related to selectivity and potency of CRF-1 antagonists. In this research investigation, we have suggests the key requirements for carbamate and aryl ether substituted pyrazinones binding to CRF-1, using an array of computational approaches, such as 2D-QSAR, 3D-QSAR, molecular docking simulations, molecular dynamics (MD) simulations, MM-GBSA binding free energy calculations, physicochemical parameter calculations. 2D and 3D-QSAR uses molecular alignment dependent technique to build a relationship between activity and compounds, statistically. Molecular docking and dynamics simulation studies analyse the residues which play a key role in binding interaction with CRF-1 protein. Molecular dynamics explored the present study by evaluation of hydrogen bond, hydrophobic interactions, ligand properties and ionic interactions. To evaluate pharmacokinetic and therapeutic profile, we performed the physicochemical parameters calculations of selected derivatives.

We hope the result obtained from this work would be useful in the identification of potential pharmacophoric and structural features involving in the binding process and in describing further insights into the essential structural modifications for the rational design and development of new potent and selective molecules as CRF-1 receptor antagonists for stress related disorders.

2. Materials and methods

An entire computational calculation was performed on Windows 7 (64-bit) operating systems with 4 GB RAM and 2.66 GHz Intel® Core™ 2 Quad Q8400 processor except molecular dynamics. Molecular dynamics simulations were performed on Ubuntu 14.04.5 version in linux environment with 4 GB RAM by Desmond. QSAR modelling was carried out by VLife Molecular Design Suite[1] (VLife MDS; Supplied by VLife Science technologies, Pune, India). The energy-minimized 3D structures were generated automatically by the VlifeEngine tool of VLifeMDS using MMFF force field with default 0.01 as RMS gradient (Friesner et al., 2004). Molecular docking, molecular dynamics simulation and binding energy calculations were carried out by Maestro, v10.4, Schrödinger software (Schrödinger, LLC, New York, 2015).

2.1 Data set collection

The 27 carbamate and aryl ether substituted pyrazinone derivatives with antagonistic activity of the CRF-1 receptor were selected for the study (Ahuja et al., 2016). The antagonistic activity (IC_{50}) was converted into negative logarithmic value (pIC_{50}). In both 2D and 3D-QSAR studies, pIC_{50} value was set as the dependent variable in all models. Chemical structures and activity of the compounds were described in Table 1.

Table 1: 2D structure, experimental and predicted activity of the compounds in 2D and 3D-QSAR

Com. Code	Structure	IC_{50} (nm)	pIC_{50}				
			Exp. value	2D-QSAR		3D-QSAR	
				Predicted value	Residual value	Predicted value	Residual value
8	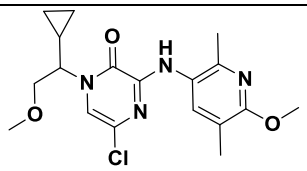	1.5	8.82	8.29	0.53	9.17	-0.35
10	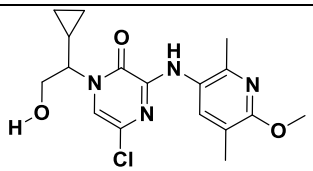	88	7.05	7.06	-0.01	7.92	-0.87
11a	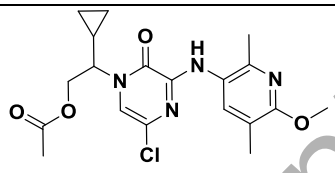	5.3	8.27	8.26	0.01	7.98	0.29
11b	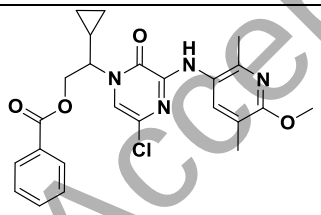	1.5	8.82	8.80	0.02	9.17	-0.35
11c	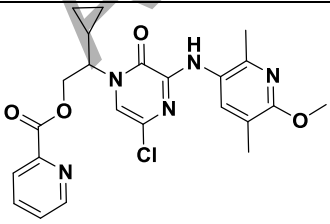	67	7.17	7.26	-0.09	8.29	-1.12

11d	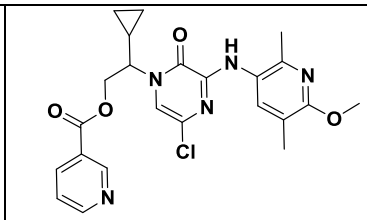	5.2	8.28	8.50	-0.22	8.56	-0.28
11e	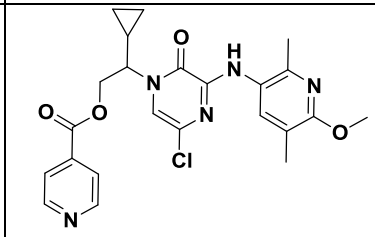	4.9	8.30	8.07	0.23	8.55	-0.25
11f	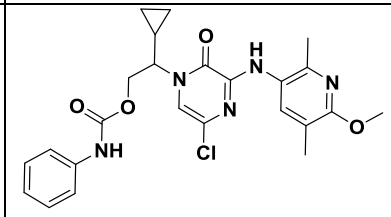	1.5	8.82	8.80	0.02	8.78	0.04
11g	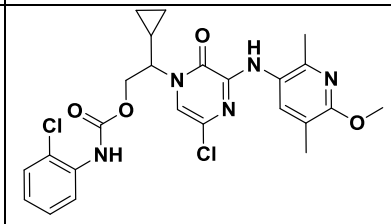	1.5	8.82	8.85	-0.03	8.53	0.29
11h	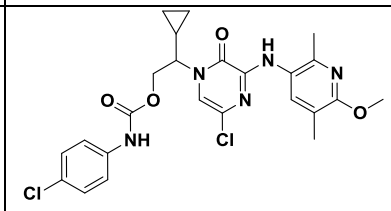	1.6	8.79	8.68	0.11	8.76	0.03
11i	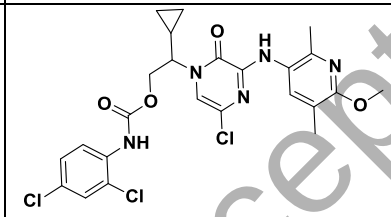	1.7	8.76	8.75	0.01	8.75	0.01
11j	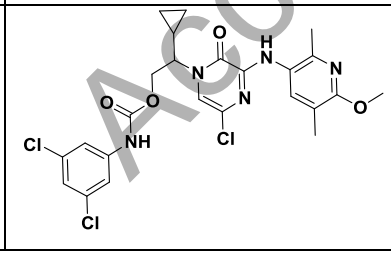	1.7	8.76	8.79	-0.03	8.80	-0.04

11k	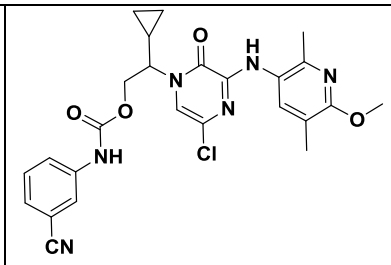	1.3	8.88	8.83	0.05	8.78	0.10
11l	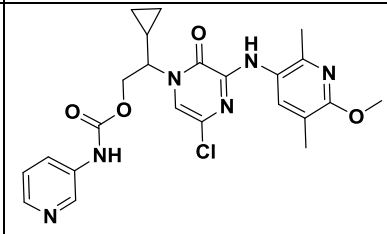	10	8.0	8.08	-0.08	8.06	-0.06
11m	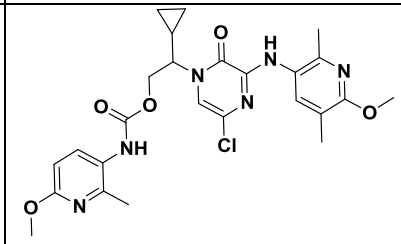	9.2	8.03	7.91	0.12	8.56	-0.53
11n	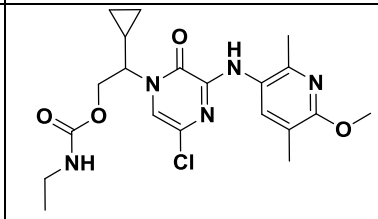	14	7.85	7.70	0.15	8.13	-0.28
11o	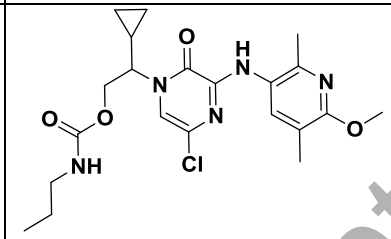	10	8.0	8.08	-0.08	8.06	-0.06
11p	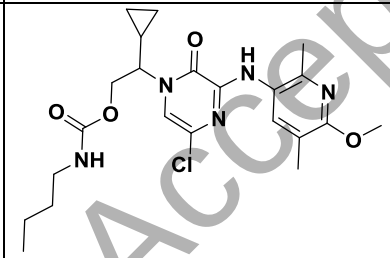	4.7	8.32	8.41	-0.09	8.41	-0.09
11q	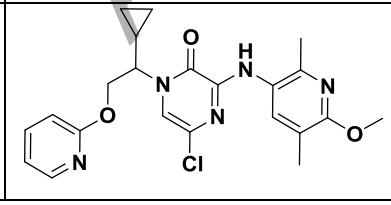	1.2	8.92	8.87	0.05	8.87	0.05

11r	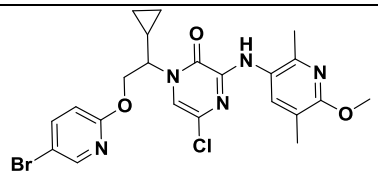	1.5	8.82	9.38	-0.56	8.17	0.65
11s	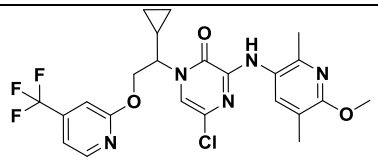	1.6	8.79	8.46	0.33	8.16	0.63
11t	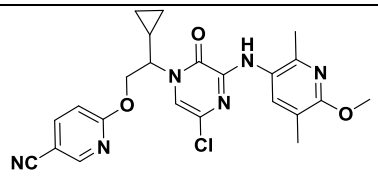	6.8	8.16	8.35	-0.19	8.08	0.08
11u	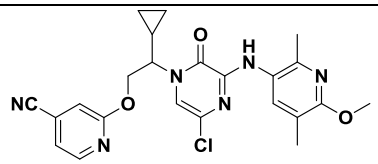	7.7	8.11	8.25	-0.14	8.06	0.05
11v	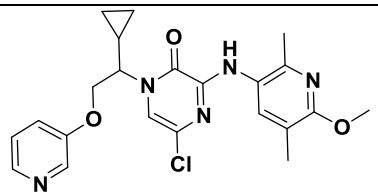	6.7	8.17	8.07	0.1	8.01	0.16
12	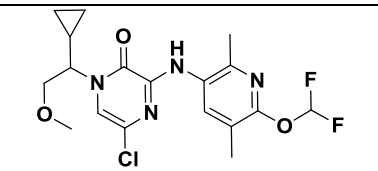	0.29	9.53	9.52	0.01	8.64	0.89
13a	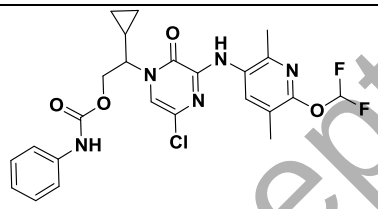	0.74	9.13	9.44	-0.31	8.54	0.59
13b	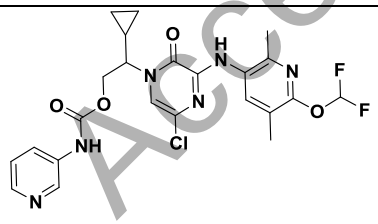	1.9	8.72	8.70	0.02	8.78	-0.06

Residual activity = Experimental activity – Predicted activity

2.3 QSAR modelling

To achieve pharmacophore identification, we performed robust 2D and 3D-QSAR studies through VLife MDS.

2.3.1 2D-QSAR

Several different regression models, viz., partial least square regression, multiple regression and principal component regression models were applied to obtain a statistically best significant model for selected datasets. To achieve QSAR equation, physicochemical and alignment independent 2D descriptors were calculated in the 2D-QSAR module. Invariable descriptors were removed due to constant for each data-point through remove invariable column option. Further to obtain QSAR model, the data set was divided into test set and training set in the advanced data selection wizard by selecting pIC_{50} value as dependent variable and remaining descriptors as independent variables. Twenty two compounds were selected as training set and remaining five compounds as a test set by manual selection method in the ratio of 1:3 (Golbraikh and Tropsha, 2000).

Test and training data set selection was validated by uni-column statistics. Uni-column statistics suggests that the min and max values in both train and test set should be compared in a way such that-

- The max of the test should be less than or equal to max of train set
- The min of the test should be greater than or equal to min of train set

According to results, the test set was interpolative and derived within the max-min range of training set that indicates the test and the training set selection was right and fit for regression model analysis.

Multiple linear regression (MLR) method coupled with the simulated annealing model was applied for obtaining best 2D-QSAR model with default the cross correlation limit as 0.5, term selection criteria as r^2, cross correlation limit as 0.5, cut off variance as 0, perturbation limit as 1 and the number of variables in the final equation as 5. MLR is the most appropriate method for multivariate data analysis and also known as ordinary least squares regression (OLS). This regression method evaluates the regression coefficient values by applying least squares curve fitting method. The regression equation obtained as in the form-

$Y = b_1*x_1 + b_2*x_2 + b_3*x_3 + c$

Where Y is the activity (dependent variable), the b_1, b_2 and b_3 are regression coefficients for corresponding x_1, x_2 and x_3 (independent variable), 'c' is a regression constant or intercept.

2.3.2 3D-QSAR

Robust 3D-QSAR study was performed in evaluating the relationship between molecular field and biological activity by using k-nearest neighbor molecular field analysis (kNN MFA)

method. kNN MFA method requires suitable alignment of a set of molecules followed by generation of common rectangular grid. So, in this intensive study, firstly most appropriate template-based alignment of all compounds was achieved by the generation of a common rectangular grid around the nucleus of all compounds with steric and electrostatic field descriptor calculation. The steric and electrostatic energies are computed at the lattice points of the grid using a methyl probe of charge +1. For steric and electrostatic field descriptor calculations, Gasteiger–Marsili was set as a charge type, dielectric constant as 1.0 with distance-dependent dielectric function. The carbon atom was selected in probe settings with charge 1.0, electrostatic and steric cutoffs selected as 10.0 and 30.0 kcal/mol, respectively. Total 2080 descriptors were computed and invariable columns were removed due to constant value and not contribute in the study.

For model development, the nineteen compounds were selected as training sets and five compounds were selected as test data sets by sphere exclusion method with 5.0 as dissimilarity value (Ajmani et al., 2006). Dissimilarity value needs to be adjusted by trial and error until a desired division of training and test set is achieved. The right data selection was analyzed by uni-column statistics and an activity distribution graph. The activity distribution graph shows that the test set compounds should lie within the range of training set compounds. The max and min of test and training set compared and found in the accepted manner. Both results indicated right data selection of training and test sets.

kNN MFA model coupled with simulated annealing variable selection method was used for generating 3D-QSAR equations. The idea of simulated annealing (SA) is to simulate a physical process called annealing in which a system is heated to a high temperature and then is gradually lowered to a preset temperature value (*e.g.* room temperature). During this process the system samples possible configurations according to Boltzmann distribution. At equilibrium low energy states will be mostly populated. Advanced parameter settings were utilized with perturbation limit set at 1, term selection criteria as q^2, cross correlation limit as 0.5, maximum temperature as 100, minimum temperature as 0.01 and iteration at given temperature as 5. Additional parameter like variance cut-off was set as 2 kcal/mol Å with auto scaling. K-nearest neighbour maximum and minimum parameters were chosen as 5 and 2 respectively, with distance based weighted average prediction method.

2.3.3Model validation

To evaluate the significance of the model, several statistical parameters such as r^2 (squared correlation coefficient), q^2 (cross-validated r^2), pred_r^2 (r^2 for external test set), se (standard error of estimate), n (number of compounds), k (number of descriptors in a model), F test (Fischer's v), df (degree of freedom), Z score (randomization test) must be taken into consideration. The value of squared correlation coefficient (r^2), cross-validated r^2 (q^2) should be greater than 0.6 and minimum standard error values of estimates establishes the quality of the model.

2.4 Molecular docking analysis

For binding mechanism prediction with target protein, molecular docking analysis was performed in addition with binding energy calculation. The most potent reported CRF-1 receptor antagonists were selected and used as references. Ligands were prepared with OPLS_2005 force field using the Ligprep tool of Schrödinger. Epic was used to generate tautomers and all possible ionization states at target pH of 7.0 ± 2.0 and also generate low energy ring conformation for each ligand. The crystal structure of CRF-1 receptor (PDB ID: 3EHT) was retrieved from Protein Data Bank (PDB) (Pioszak et al., 2008). Co-crystallized structure with CRF (PDB ID: 3EHT) having 3.4 Å resolution was prepared using protein preparation wizard by added missing hydrogen atoms, added missing atoms and loops, assigned bond orders and deleted the non binding waters. Further, the H-bond assignment using Propka (with pH 7.0) and restrained minimization was proceeded using OPLS_2005 force field to remove steric clashes of the atoms. Docking was executed followed by generation of grid (binding site) using Glide module in extra precision (XP) mode. The receptor grid box was generated 25 Å size into the binding site of the protein by removing crystallized ligand CRF. For docking, protein was set as rigid while ligands were chosen as flexible to generate conformations. Post docking minimization was proceeded to achieve conformational distinct poses. The best pose was selected and energy minimized and ranked by Glide Gscore.

2.5 Binding free energy calculation using Prime

The relative binding energies were calculated using the Prime MM-GBSA tool of Schrödinger suite with default parameters (Li et al., 2011). This tool computes ligand strain and ligand binding energies of ligand-protein complexes. The binding free energy is computed by given equation (Su and Johnson, 2016; Su et al., 2015).

$$\Delta G_{bind} = G_{complex} - (G_{protein} + G_{ligand})$$

Where, ΔG_{bind} is the binding free energy, $G_{complex}$ is free energy of complex, $G_{protein}$ is free energy of the target protein and G_{ligand} is ligand free energy.

2.6 Molecular dynamics simulations

Molecular dynamics simulation study was carried out through Desmond tool of Schrödinger for ligand-protein complex (Kevin et al., 2006). In all screened compounds, the best one was selected for MD simulations on the basis of number of hydrogen bonds, binding energy and glide score parameters. In this study, we selected compound **11i** and compound **2** (reference molecule) for simulation analysis. The simulation calculation accomplished in three steps viz. system builder, energy minimization and molecular dynamics. A solvated system was generated by selecting SPC as solvent model, POPC as membrane with orthorhombic box shape. Buffer was selected for box size calculation at distance 10.0 Å. The physiological condition of the simulation box was achieved by neutralize the charge and salt concentration was set at 0.15 M of Na^+ and Cl^- ions. The volume of the simulation box is minimized by aligning the principal axes of the solute along the box vectors or the diagonal. The solute in the solvated system contains protein, protein complex, protein-ligand complex, protein immersed in a membrane bilayer, etc. Energy of the ligand-protein complex was minimized by maximum 2000 iterations to remove steric clashes in complex. The pre-processed ligand-protein complex was loaded from work space of the MD tab and NPT ensemble was set at 300.0 K temperature and 1.01325 bar as pressure. After relaxation of model system 50 ns simulations was performed and trajectory was recorded at 4.8 ps for ligand-protein complex (Shivakumar, Williams, Wu, Damm, Shelley, Sherman, 2010). Energy, ligand-protein RMSD, RMSF, protein-ligand contacts and ligand properties were analyzed to check the conformational behaviour and stability of the complex during the 50 ns simulation.

2.7 Physiochemical properties analysis

Physicochemical parameters calculation of all compounds was performed using a QikProp module of Maestro (Goyal et al., 2014). In this module, all compounds were also analyzed for drug likeness ability which essential to be taken into account to consider designing an ideal drug.

3. Result and discussion

3.1 2D-QSAR analysis and model validation

The substituted pyrazinone compounds were selected and divided into test and training set having 5 & 22 compounds respectively for 2D-QSAR analysis. Selection of training and test sets were validated through uni-column statistics. The max of the test set is less than max of training set and min of the test set is greater than min of training set. The test set was found to be interpolative within the minimum-maximum ranges of training set along with standard deviation according to uni-column statistics (Table 2).

Table 2: Uni-column statistics results for 2D-QSAR model

	Average	**Max**	**Min**	**StdDev**	**Sum**
Activity (Training set)	8.4394	9.5300	7.0500	0.6671	143.4700
Activity (Test set)	8.2667	9.1300	7.1700	0.6840	49.6000

Validated data sets were analyzed to obtain robust 2D-QSAR model through various statistical method. The best significant model obtained through MLR method coupled with simulated annealing is given in equation 1:

pIC_{50} = (-0.35 T_T_N_2 - 0.05 T_2_T_7 – 0.01 SdOE-index + 14.67 SsssNE-index -0.87 SsClcount – 0.84 T_N_N_6 + 0.04 T_T_C_1 – 42.93 DeltaEpsilonC + 0.43 T_2_C_5 – 0.12 T_C_C_6) + (-17.69) eq. (**1**)

Other statistical significant parameters are given as:

N = 22, degree of freedom = 11, F test = 40.8149, r^2 = 0.9738, q^2 = 0.8963, r^2_se = 0.1307, q^2_se = 0.2598, pred_r^2 = 0.7267, pred_r^2se = 0.2296, Zscore_r^2 = 4.59735, Zscore_q2 = 1.77962.

The squared correlation coefficient (r^2 = 0.97) explains the quality of fit by 97% of total variance in the training set (N = 22). It also has an internal (q^2) and external (pred_r^2) predictive ability of ~89% and ~72% respectively. The F-test value shows the statistical significance of the model, approximately, 99.99% which means that the probability of failure of the model is 1 in 10000. Zscore is calculated by a randomization test (Table 3).

Table 3: Randomization test results for 2D-QSAR (MLR model)

Dependent variable	Z Score r^2	Z Score q^2	Best Rand r^2	Best Rand q^2	Alpha Rand r^2	Alpha Rand q^2	Z Score Pred r^2	Best Rand Pred r^2	Alpha Rand Pred r^2
Activity	4.59735	1.77962	0.74098	0.45480	0.00008	0.05000	0.91086	0.62405	0.00000

The randomization test shows confidence of ~ 99.9 % that the generated model is not random and so it is selected as the QSAR model. A high r^2 and low standard error r^2 (r2_se) value of 0.9738 and 0.1307 denotes the accuracy of the obtained model. These parameters proved that generated model is robust for 2D-QSAR and have excellent correlation between activity and descriptors.

The fitness plot (Figure 2) for observed vs. predictive activity provides an idea about how well the model was trained and how well it predicts the activity of the external test set. This plot describes the dependence of pIC_{50} on various types of geometrical and topological descriptors. In this plot points were near to regression line that shows true prediction of training set activity along with external test set.

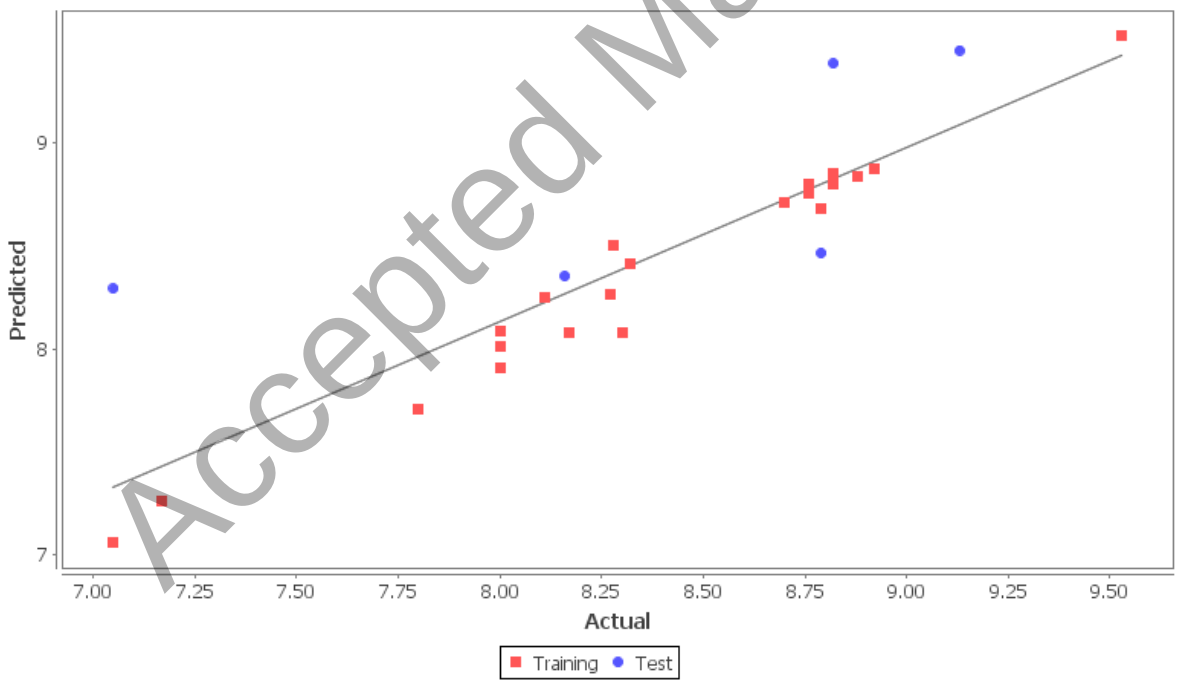

Figure 2: Fitness plot for observed vs. predictive activity

A radar plot (Figure 3) of test and training set was also generated to depict the closeness between actual and predicted activity for both test and training sets due to extent of overlapping. The red colour indicates actual activity and blue for predicting activity of the compounds.

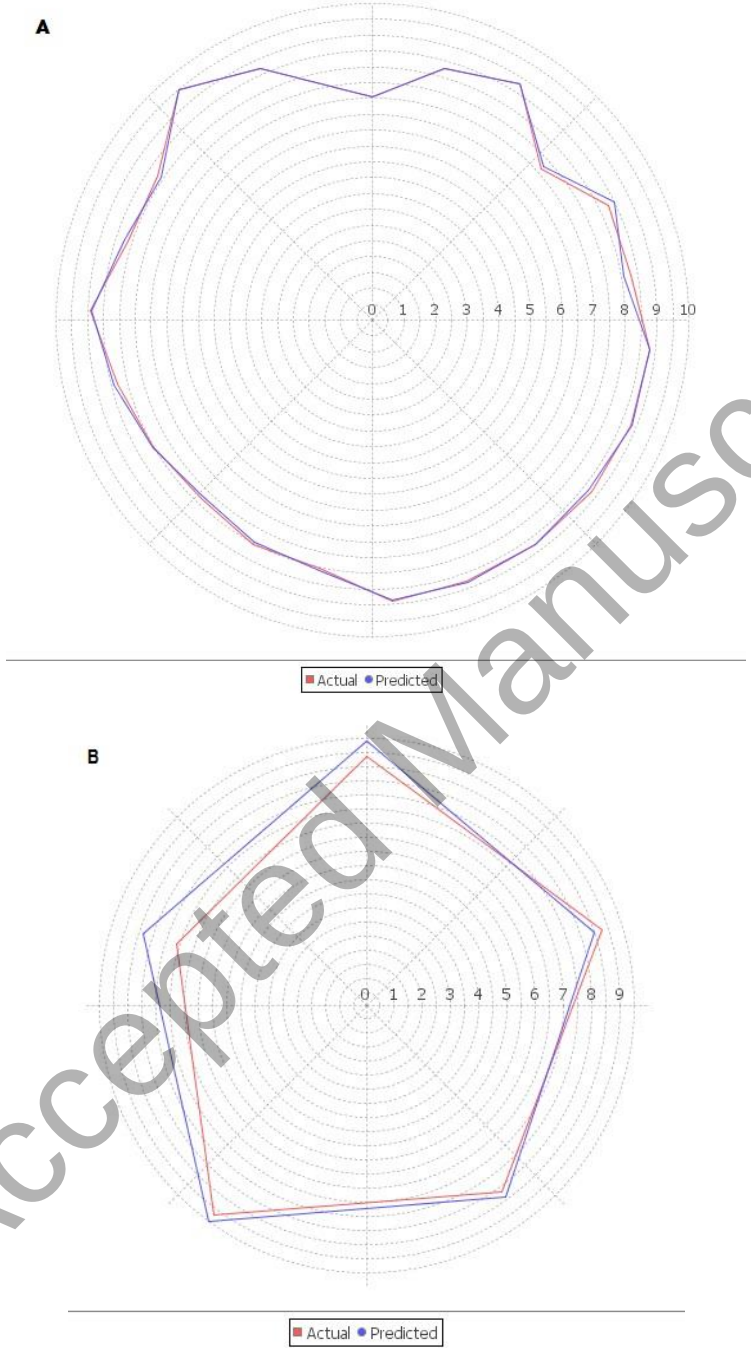

Figure 3: Radar graph for depiction of actual and predicted activities **A)** Training set **B)** Test set

3.2 Contribution of 2D descriptors

The obtained MLR model revealed that the descriptors T_T_N_2, T_2_T_7, SdOE-index, SsssNE-index, SsClcount, T_N_N_6, T_T_C_1, T_C_C_6 , T_2_C_5, DeltaEpsilonC plays most important role in predicting activity which explains the correlation with standard to the variation in various substitution sites (Figure 4).

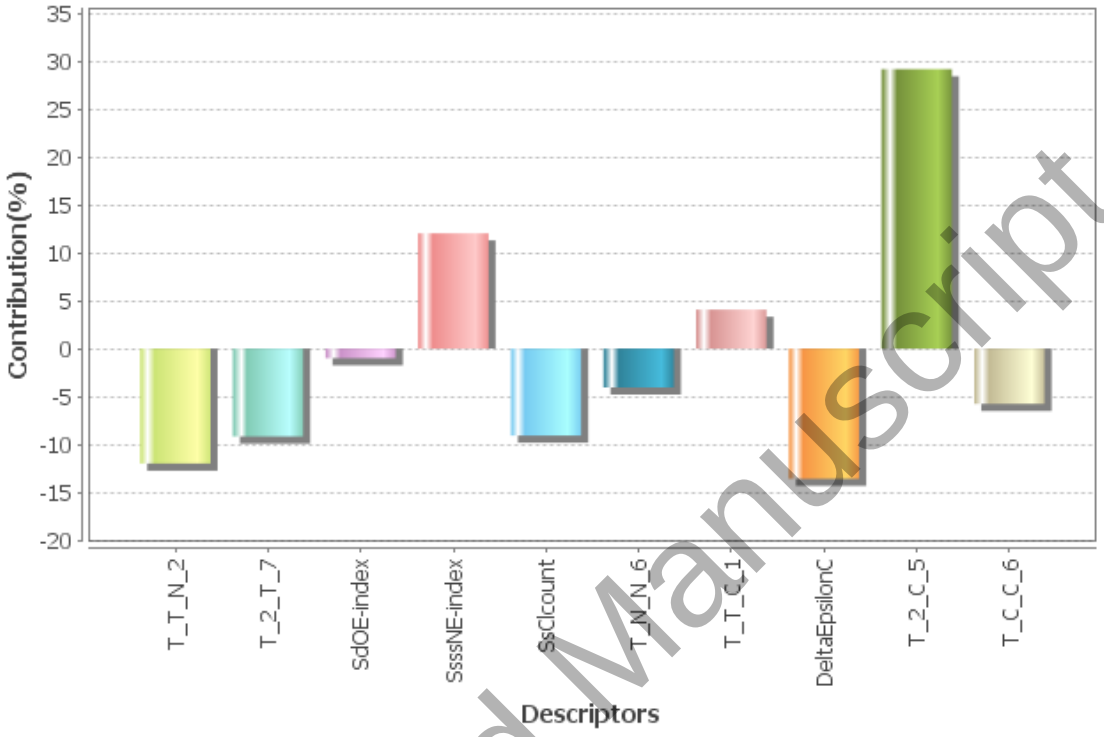

Figure 4: Contribution plot of 2D descriptors

T_T_N_2: This alignment independent descriptor is the count of the number of atoms (single, double or triple bonded) separated from nitrogen atom by 2 bonds. This descriptor shows negative contribution in terms of percentage is 12%.

T_2_T_7: This descriptor describe about the topology of the molecule. It revealed that the count of number of double bonded atoms (*i.e.* any double bonded atom, T_2) separated from any other double bonded atom by 7 bonds in a molecule. The negative contribution of the descriptor in percentage is 10%.

SdOE-index: This electro topological state index indicates the number of oxygen atom connected with one double bond. The negative contribution of the descriptor in percentage is 2%.

SsssNE-index: This electro topological state index indicates the number of nitrogen atom connected with three single bonds. The positive contribution of the descriptor in percentage is 12%.

SsClcount: This physiochemical descriptor defines the total number of chlorine atom connected with one single bond. The percentage of contribution of descriptor is 10% (negative contribution). This suggests that less substitution with chlorine atom enhance the activity.

T_N_N_6: This alignment independent descriptor indicates that the count of number of nitrogen atoms (single, double or triple bonded) separated from any other nitrogen atom (single, double or triple bonded) by 6 bonds in a molecule. The percentage of contribution of descriptor is 5% (negative contribution).

T_T_C_1: This alignment independent descriptor is the count of the number of atoms (single, double or triple bonded) separated from carbon atom by 1 bond. This descriptor shows positive contribution in terms of percentage is 5%.

T_C_C_6: This is the count of number of carbon atoms (single, double or triple bonded) separated from any other carbon atom (single double or triple bonded) by 6 bond distance in a molecule. The percentage of contribution of descriptor is 5% (negative contribution).
T_2_C_5: This is the count of number of double bounded atoms (*i.e.* any double bonded atom, T_2) separated from carbon atom by 5 bonds. The percentage of contribution of descriptor is 30% (positive contribution).

DeltaEpsilonC: This topo-chemical atom based descriptor is a measure of contribution of electronegativity. The negative contribution of the descriptor in percentage is 15% that indicates electronegativity decreases the activity.

A selective distance count statistic counts all the fragments between start atom with attribute (0 to 7) and end atom with attribute (0 to 7) separated by the graph distance 3. The graph distance can be defined as the smallest number of atoms along the path connecting two atoms in the molecular structure. The experimental and predicted activities of analysed compounds with their calculated residual activity values are described in Table 1.

3.3 3D-QSAR model validation

An intensive 3D-QSAR study was performed by applying k-nearest neighbor molecular field analysis (kNN MFA) method coupled with the simulated annealing method. All compounds were again divided into test and training sets through sphere exclusion method with dissimilarity value 5.0. The data selection was validated through uni-column statistics. According to the uni-column statistics results (Table 4), the max of the test set is less than the max of training set and min of the test set is greater than min of training set, which indicates the right data selection.

Table 4: Uni-column statistics results for 3D-QSAR model

	Average	**Max**	**Min**	**StdDev**	**Sum**
Activity (Training set)	8.4060	9.5370	7.0550	0.5296	159.7140
Activity (Test set)	8.5488	9.1300	7.1730	0.7813	42.7440

Finally, kNN MFA model coupled with simulated annealing (SA) was applied by generation of a common rectangular grid around the nucleus. The advanced parameters were set as previously as in 2D-QSAR. The best model suggests that electrostatic interactions (E_322, E_815, E_307, and E_89) and steric interactions (S_966, S_244, S_350, S_592, S_447, and S_420) play a vital role in the determination of biological activity. The descriptors along with range and other statistical parameters are given as:

k Nearest Neighbour = 2, N = 19, degree of freedom = 8, q^2 = 0.5253, q^2_se = 0.3649, pred_r^2 = 0.7776, pred_r^2se = 0.0492.

Descriptors with range = E_322: -0.0550 to -0.0160

E_815: -0.9210 to -0.6180

E_307: -0.1450 to 0.4040

E_89: 0.0630 to 0.0940

S_966: -0.1440 to -0.0810

S_244: -0.0320 to -0.0250

S_350: -0.1520 to 0.6540

S_592: -0.5700 to -0.5590

S_447: -0.2270 to -0.2000

S_420: -0.0040 to -0.0040

Statistically, the obtained model is comparatively better with respect to the internal (q^2 = 0.5253) as well as the external (pred_r^2 = 0.7776) model validation and accurately predicts the activity ~52% and ~77% for the training and test set respectively.

The experimental and predicted activities of analysed compounds are given in Table 1 with their residual activity value. The difference between observed vs. predictive activity in distance point terms is shown in Figure 5. This fitness plot explains the dependence of activity on different kind of the descriptors and provides the information about how well the model was trained and how well it predicts the activity of external set.

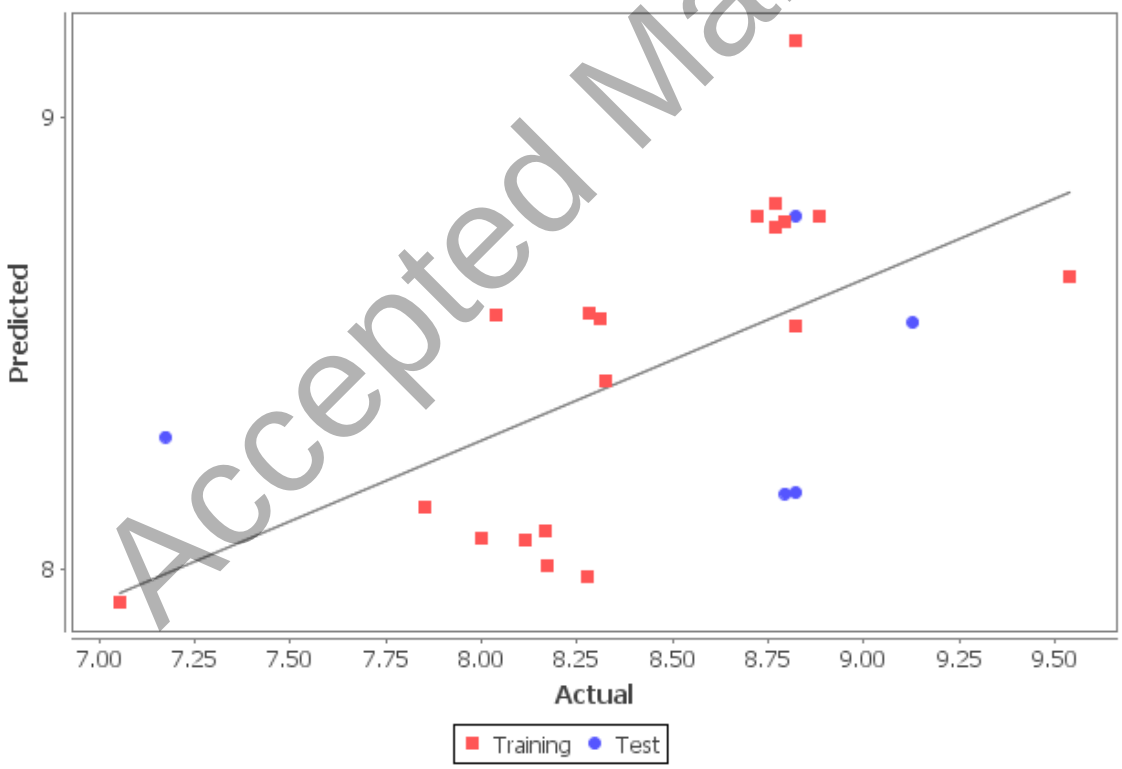

Figure 5: Fitness plot for observed and predicted activity

3.4 3D-QSAR interpretation and pharmacophore identification

The descriptors that get selected in the given model are the field points which uses 4 electrostatic and 6 steric field descriptors along with its 2 k nearest neighbour (k = 2) to evaluate the activity of new molecules. Figure 6 shows the position and ranges of the corresponding electrostatic and steric fields in the kNN MFA model provides the information for the design of new molecules. 3D plot of the kNN MFA which shows the relative position and ranges of the corresponding important electrostatic and steric fields in the model provides the following guidelines for the design of new molecules.

1. For electrostatic field, negative range indicates that negative electrostatic potential is favourable for an increase in the activity and hence a more electronegative substituent group is preferred in that region, whereas positive range indicates that positive electrostatic potential is favourable for an increase in the activity and hence a less electronegative substituent group is preferred in that region.

2. For steric field, negative range indicates that negative steric potential is favourable for an increase in the activity and hence less bulky substituent group is preferred in that region whereas positive range indicates that positive steric potential is favourable for an increase in the activity and hence more bulky substituent group is preferred in that region.

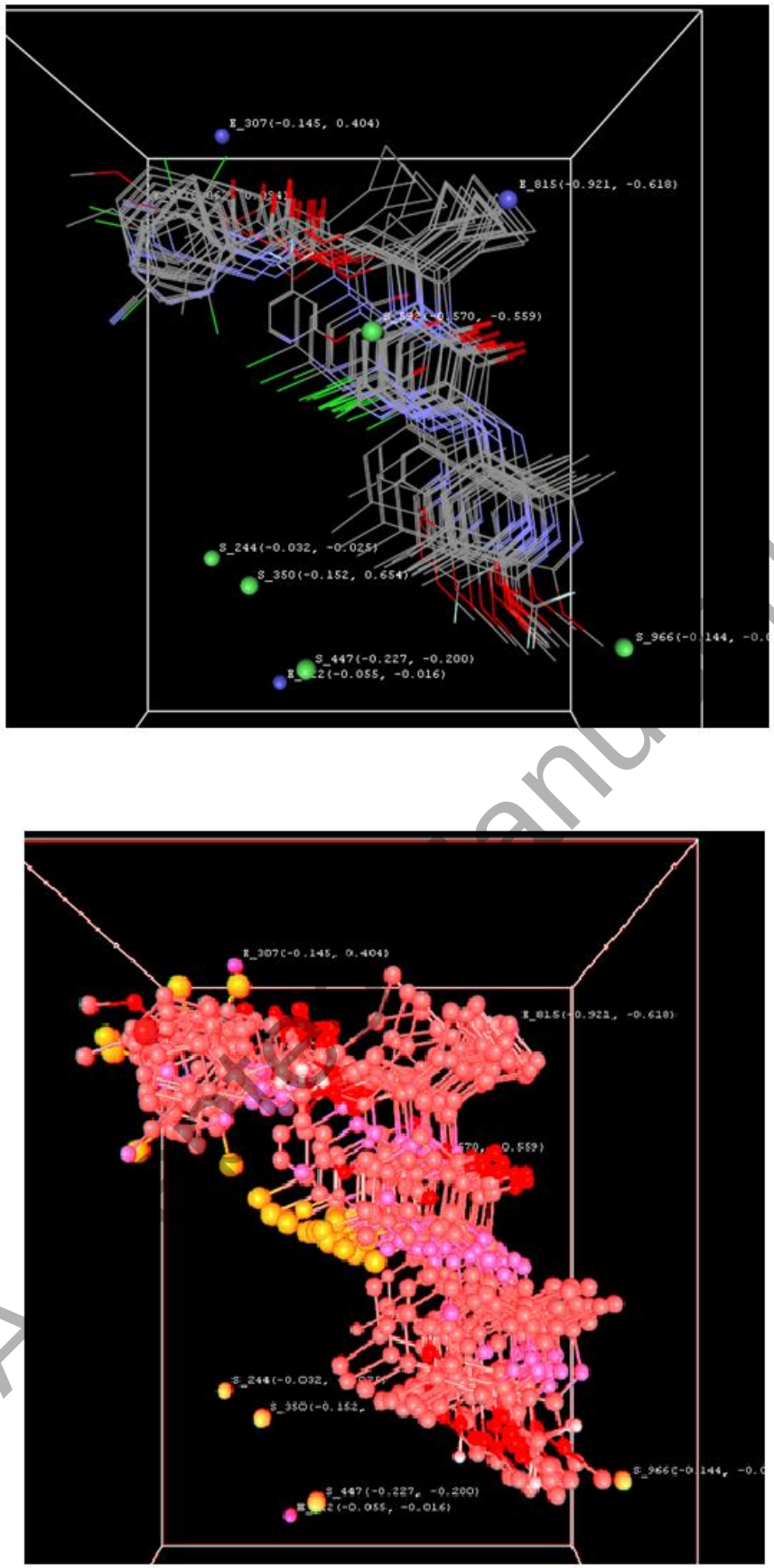

Figure 6: 3D plot of rectangular grid around the selected compounds through kNN-MFA method

According to these guidelines and developed SW-kNN MFA model field plot, 3 electrostatic fields range (E_322, E_815, and E_307) shows the ranges are more towards the negative side, and hence, increasing electronegativity of the substituent group is favourable at the pyrazinone core. While 1 electrostatic field range descriptor E_89 shows the range is towards the positive side, meaning the presence of electropositive group such as methyl, ethyl, propyl, butyl and isopropyl group enhance the activity. Same as, all steric fields range S_966, S_244, S_350, S_592, S_447 and S_420 shows the range towards negative side that indicates the presence of less bulky substituent increases the activity.

Thus, in the context of 2D and 3D-QSAR investigation, the structural requirement for more potent antagonistic activity is analysed. The study revealed that the nitrogen substituted carbamate are essential for antagonistic activity and also increase the lipophilicity. Compound **13a** with nitrogen substituted carbamate has the highest biological activity as compared to compounds **11a**, **8** and **10** due to lack of nitrogen at carbamate site. Substitution with an aromatic ring such as phenyl, pyridyl at carbamate site enhance the activity. Therefore, pharmacophore of the synthesized compounds were obtained and given in figure 7.

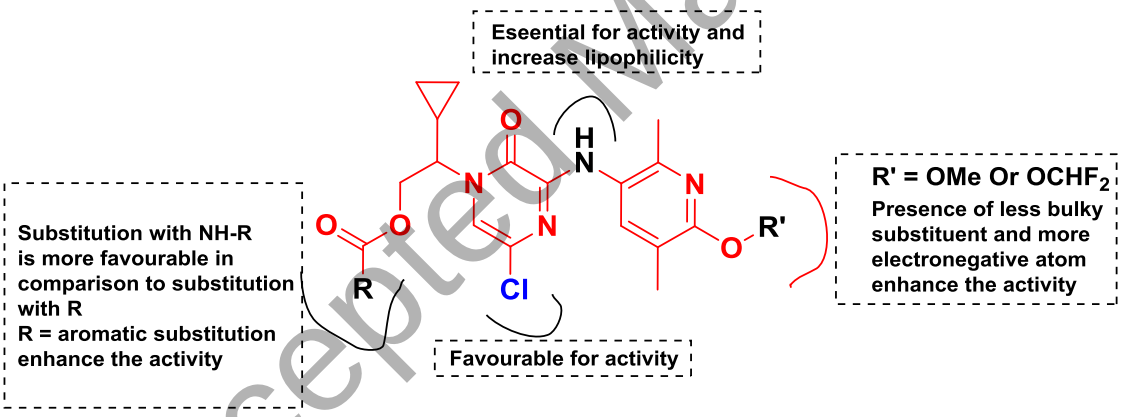

Figure 7: Structure activity relationship by intensive QSAR study

3.5 Molecular docking studies

To explore the investigation, we performed molecular docking analysis of all compounds with reference compounds. The co-crystallized receptor protein (PDB ID: 3EHT) has been selected for performing docking. The grid was generated around the binding site of protein, prior to docking. The docking results with binding energy calculation were revealed in the Table 5.

Table 5: Glide docking score along with binding energies of compounds and reference compounds

Com. Code	Glide Gscore	dG Bind	dG Bind Coulomb	dG Bind Lipo	dG Bind Hbond	dG Bind vdW
8	-5.695	-55.824	1.681	-46.674	-0.226	-40.987
10	-7.407	-34.097	-16.154	-25.582	-0.581	-29.878
11a	-6.790	-52.932	-8.814	-29.052	-0.873	-31.115
11b	-6.055	-46.324	-3.741	-30.510	-0.469	-35.043
11c	-6.510	-68.174	-5.627	-23.560	-0.199	-38.118
11d	-6.528	-61.040	-3.679	-30.044	-0.391	-35.836
11e	-7.698	-59.469	-15.102	-29.709	-0.387	-35.692
11f	-8.904	-72.970	-13.697	-21.264	-0.677	-34.673
11g	-9.392	-85.541	-1.550	-22.759	-1.09	-34.554
11h	-9.140	-66.474	-4.118	-29.508	-0.388	-36.816
11i	-9.809	-82.224	-2.038	-29.739	-0.398	-37.402
11j	-6.294	-81.238	-6.746	-40.996	-0.873	-49.346
11k	-9.392	-48.334	-17.387	-26.161	-0.636	-40.748
11l	-7.959	-79.865	-11.495	-27.071	-1.298	-38.990
11m	-5.895	-59.160	-17.491	-27.307	-0.669	-42.123
11n	-6.634	-65.982	-10.223	-29.254	-0.722	-33.969
11o	-6.364	-54.797	-4.082	-24.590	-1.577	-31.763
11p	-6.785	-57.597	-14.535	-18.039	-1.368	-29.203
11q	-6.246	-57.265	-1.226	-29.233	-0.251	-37.042
11r	-6.465	-48.606	-7.736	-28.084	-0.349	-34.698
11s	-5.777	-31.570	-6.739	-19.742	-1.030	-35.306
11t	-5.581	-33.946	0.223	-25.880	-0.458	-37.926
11u	-6.528	-44.736	-10.449	-19.142	-1.180	-29.274
11v	-5.820	-43.961	-2.807	-49.271	-0.308	-47.130
12	-7.022	-39.872	-10.544	-26.676	-0.458	-30.440
13a	-5.089	-57.975	-10.937	-30.641	-0.687	-38.025
13b	-8.359	-78.891	-7.112	-24.515	-1.418	-35.407
1	-4.771	-34.352	-5.751	-15.625	-0.597	-28.712
2	-7.844	-66.009	49.797	-18.466	-0.289	-29.435
3	-8.287	-77.276	-1.164	-26.439	0.000	-26.846
4	-4.105	-42.783	-7.389	-20.936	-0.261	-29.052
5	-4.917	-49.987	-16.524	-20.406	-0.325	-27.718
6	-6.089	-39.318	8.356	-19.135	-0.557	-33.808
7	-2.548	-42.479	-7.542	-25.201	-0.344	-31.327

9	-7.327	-28.029	-11.844	-25.928	-0.417	-31.181

Compound **11i** (2-(5-chloro-3-((6-methoxy-2,5-dimethylpyridin-3-yl)amino)-2-oxopyrazin-1(2*H*)-yl)-2-cyclopropylethyl (2,4-dichlorophenyl)carbamate) has the highest docking score -9.809 and shows 3 hydrogen bonds with residue Asp284 and Asp335. It also shows one π-π stacking interaction with Trp9. In reference compounds, compound **3** has the highest docking score -8.287 and shows one π-π stacking interaction with Trp9 and one π-cation interaction with Tyr194. The interesting fact is that most of the synthesized compounds show hydrogen bonding with same amino acid Asp284 and Glu305 with different bond distance. The ligand interaction diagram and 3D structures of docked ligands are given in figure 8 and 9 respectively.

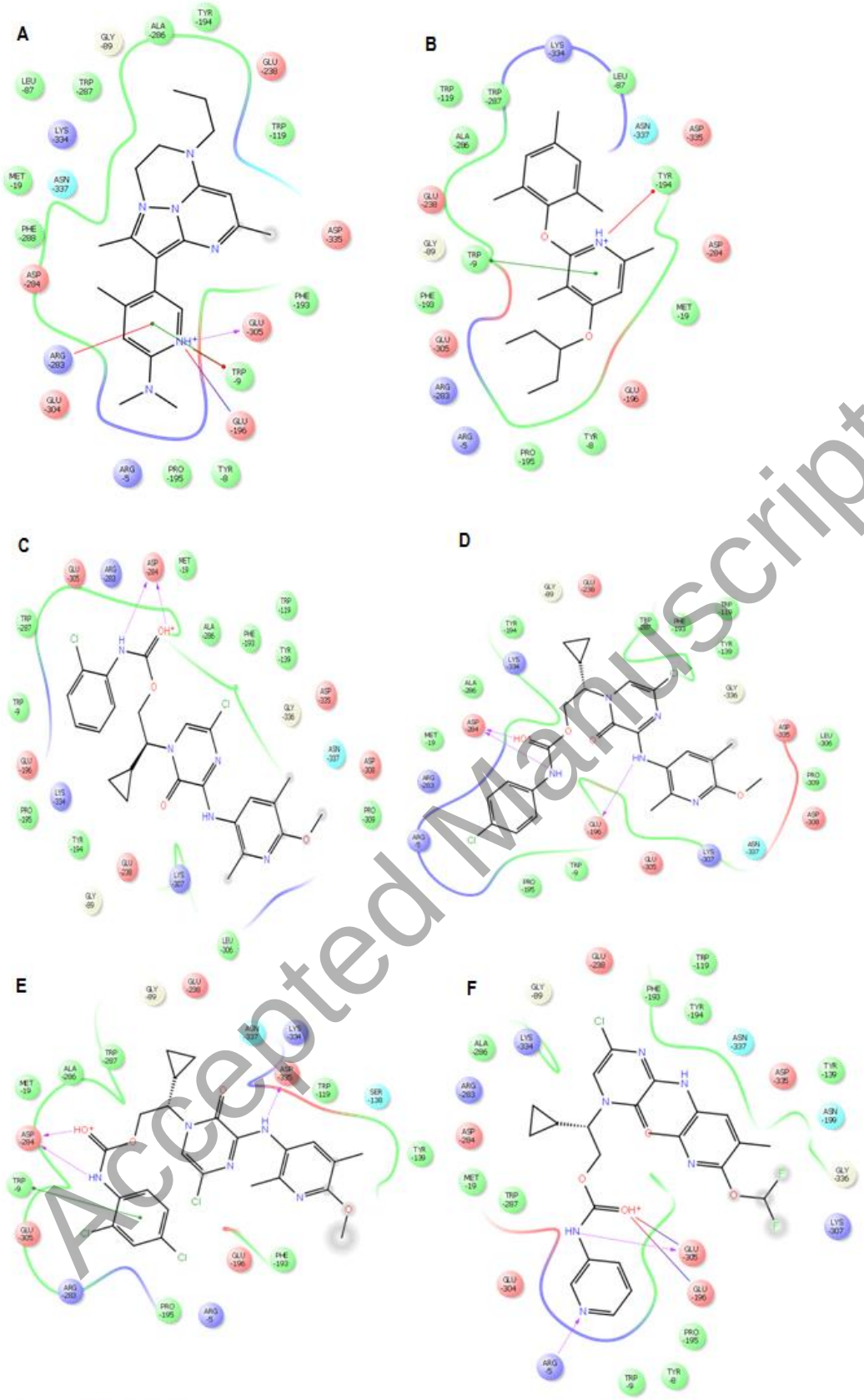

Figure 8: Target protein-ligand interaction diagram (A) Compound **2** (B) Compound **3** (C) Compound **11g** (D) Compound **11h** (E) Compound **11i** (F) Compound **13b**

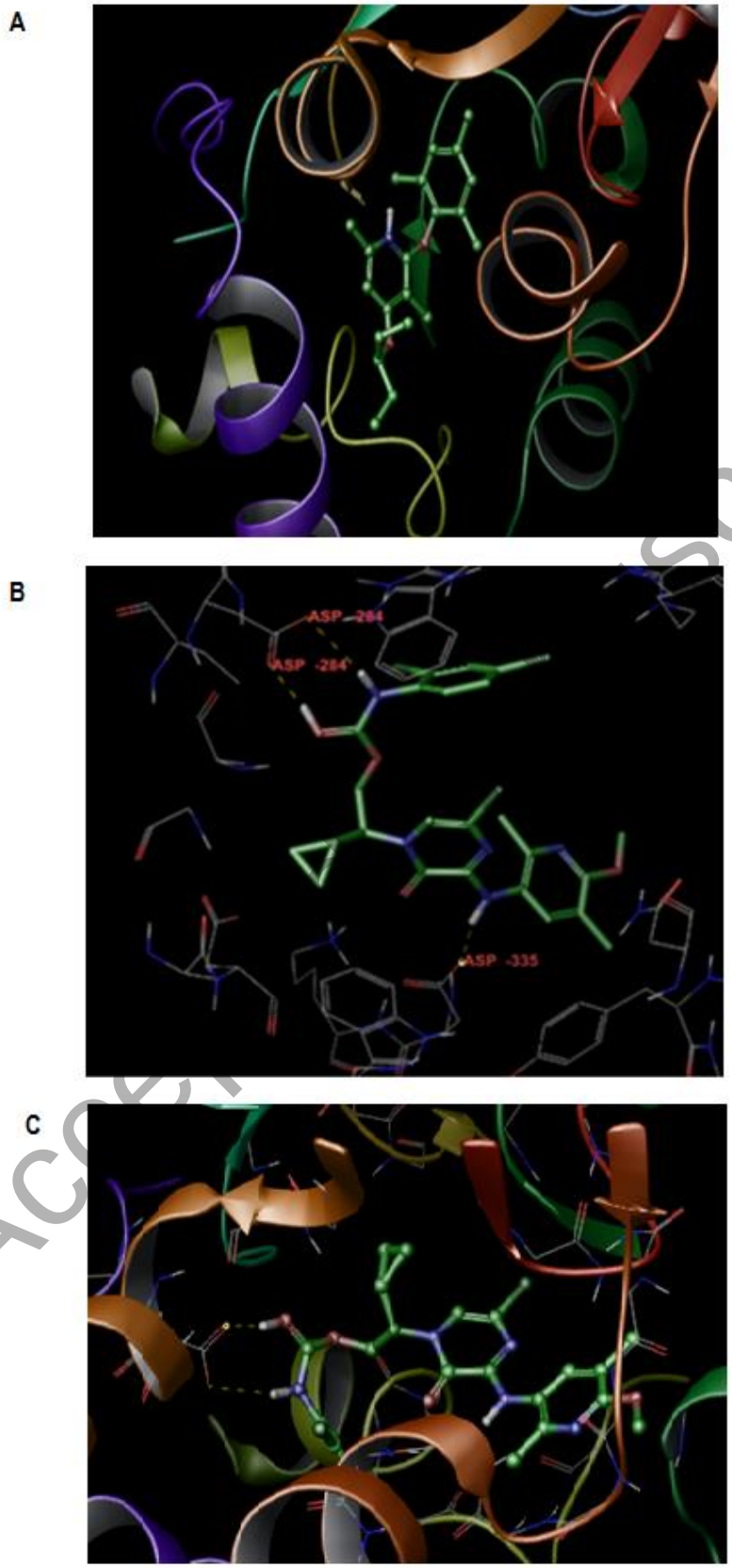

Figure 9: (A) Binding view of reference compound **3** (B) Hydrogen bond interaction of compound **11i** (C) Binding view of compound **11g** with hydrogen bonds

Overall, Compound **11i** has highest binding affinity towards target protein. The docking results revealed that the binding residue Phe193, Tyr194, Trp119, Tyr139, Pro195, Tyr8, Trp9, Trp287, Met19, Phe288, Ala286 consists hydrophobic region of the protein and responsible for hydrophobic interaction with compounds. More hydrophobic interactions enhance the binding affinity (Patil et al., 2010). Therefore, comparison of synthesized compounds with reference molecules suggests that aromatic substitution at carbamate nitrogen shows excellent binding due to π-π stacking interaction. Large bulky groups do not contribute in binding as well as activity. According to the ligand interaction diagram, the binding pocket consists of ten hydrophobic (Phe193, Tyr194, Trp119, Tyr139, Pro195, Tyr8, Trp287, Met19, Phe288, and Ala286), two hydrogen bonding (Asp284, Glu305) and one π-π stacking (Trp9) amino acid residues.

3.6 Molecular dynamics results

This simulation study was performed on top scored compound **11i** and reference compound **2** which qualifying all parameters using Desmond tool. The neutralization of both ligand-protein complexes was accomplished with 5 Cl- ions and the overall ions of complex were found 11 Na+ and 16 Cl- ions. Prior to molecular simulation studies, system was minimized with 2000 iterations. The structural stability of protein-ligand complex were assessed by root mean square deviation (RMSD) which denotes the measure in the average change in displacement of a selection of atoms for a particular frame with respect to a reference frame (Kumar et al., 2016). The RMSD of compound **11i** and compound **2** for 50 ns was found to be 6.0 Å and 7.1 Å respectively. For compound **11i**, it indicates that the protein is undergoing a large conformational change during the simulation, while for reference compound **2**, protein exhibit large convergence (Figure 10).

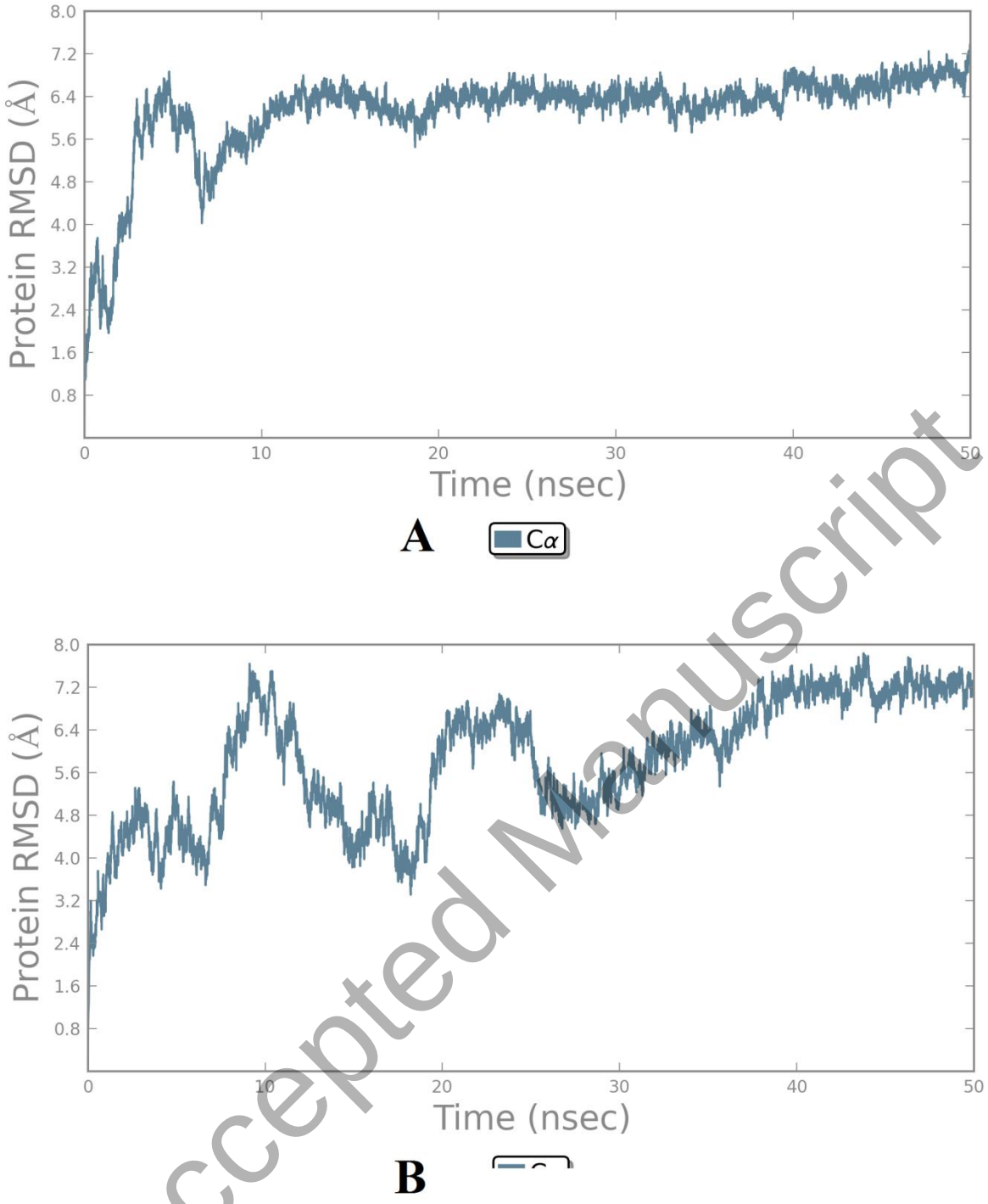

Figure 10: RMSD of ligand-protein complex (A) Compound **11i** (B) Compound **2**

A root mean square fluctuation (RMSFs) is another useful parameter for characterizing flexibility of different regions of protein as well as local changes along the protein chain. For compound **11i**, RMSF of protein residues was found to be 2.4 Å and lies below from 5.6 Å where as in compound **2**, RMSF lies below 10.5 Å. It suggests large conformational changes in C-terminal and N-terminal residues.

The ligand-protein interactions were observed during simulation process and depicted in Figure 11. Ligand-protein interactions (or 'contacts') are categorized into four types: Hydrogen Bonds, Hydrophobic, Ionic and Water Bridges. Hydrogen bonding plays a significant role in ligand binding due to strong influence on drug specificity, metabolism and adsorption. In compound **11i** (2-(5-chloro-3-((6-methoxy-2,5-dimethylpyridin-3-yl)amino)-2-oxopyrazin-1(2*H*)-yl)-2-cyclopropylethyl (2,4-dichlorophenyl)carbamate), hydrogen bonding has been observed with Asp-335, Lys-334, Asp-284 and Tyr-139. The residues involved in hydrophobic interactions were Trp-287, Ala-286, Tyr-194, Tyr-139, Trp-119, Met-19 and Trp-9. An ionic interaction with Lys-334 residue has been observed. In reference compound **2** (3-(6-(dimethylamino)-4-methylpyridin-3-yl)-2,5-dimethyl-*N*,*N*-dipropylpyrazolo[1,5-a]pyrimidin-7-amine), the amino acid residue Glu-305, Glu-135, Trp-119 and Lys-52 involved in hydrogen bonding in very less fractions. Beside this, the water contacts were also seen.

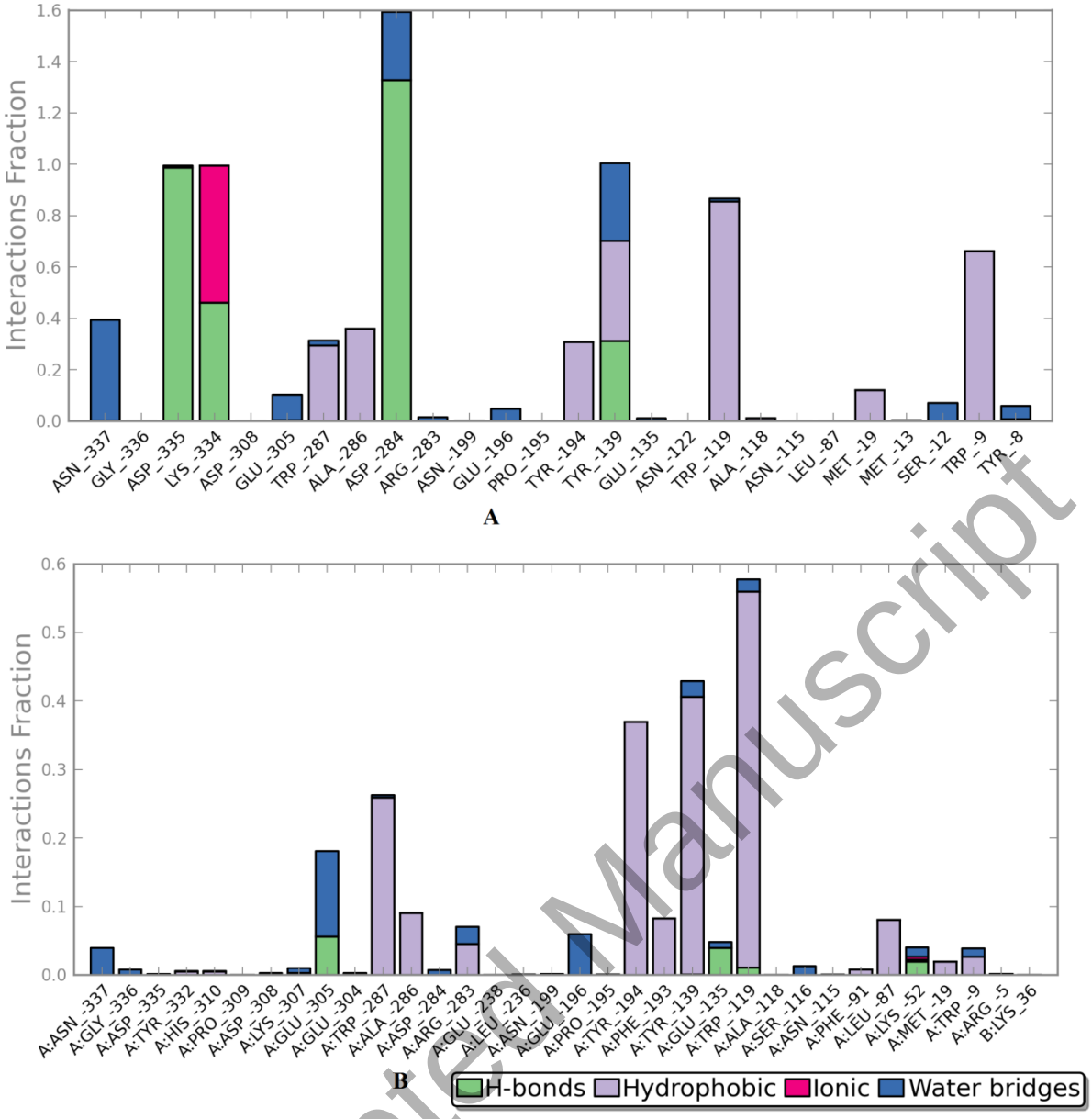

Figure 11: Ligand-protein interactions (A) Compound **11i** (B) Compound **2**

3.7 Physiochemical properties

All synthesized compounds with reference compounds were subjected to evaluate their physicochemical parameters by using Qikprop tool of the maestro. Principle and therapeutic significant parameters are given in table 6 and 7 respectively. The QPlogPo/w value is used to calculate the lipophilic efficiency that measures the potency of drug. Therefore Octanol-water partition coefficient logP value is essential in rational drug design and QSAR studies. Polar surface area (PSA) is the sum of all polar atoms mainly oxygen and nitrogen including attached hydrogen. A molecule which have more number of rotatable bond (rotor) become more flexible and have good binding affinity with binding pocket (Sharma et al., 2016).

Table 6: Principle pharmacokinetic parameters of selected compounds

Com. Code	MW	dipole	donorHB	accptHB	volume	rotor	PSA
8	378.858	2.236	0.25	6.45	1184.32	7	72.753
10	366.847	3.218	1.25	6.45	1127.595	7	81.825
11a	406.868	2.628	0.25	6.75	1256.978	7	100.668
11b	468.939	6.514	0.25	6.75	1425.998	8	92.777
11c	469.927	3.789	0.25	7.75	1440.181	8	107.518
11d	469.927	3.945	0.25	8.25	1390.789	8	109.559
11e	469.927	3.741	0.25	8.25	1435.71	8	111.215
11f	483.953	3.083	1.25	7.25	1499.613	8	108.599
11g	518.399	5.795	1.25	7.25	1504.768	8	105.638
11h	518.399	7.718	1.25	7.25	1522.21	8	107.172
11i	552.844	5.195	1.25	7.25	1545.994	8	99.324
11j	552.844	6.442	1.25	7.25	1562.301	8	101.595
11k	508.963	8.586	1.25	8.75	1500.82	9	123.939
11l	484.941	7.504	1.25	8.75	1454.71	8	118.521
11m	528.994	6.474	1.25	8.25	1600.66	9	125.547
11n	435.909	4.381	1.25	7.25	1354.446	8	111.08
11o	449.936	4.637	1.25	7.25	1355.839	9	107.681
11p	463.963	2.176	1.25	7.25	1467.014	10	107.991
11q	443.932	4.878	0.25	5.75	1377.165	8	79.686
11r	522.828	5.138	0.25	5.75	1379.802	8	77.004
11s	511.93	4.425	0.25	5.75	1392.817	8	76.833
11t	468.942	6.536	0.25	7.25	1447.053	9	102.554
11u	468.942	7.044	0.25	7.25	1392.627	9	106.484
11v	443.932	3.302	0.25	7	1323.381	8	83.812
12	380.873	2.944	0.25	6.45	1182.449	7	69.817
13a	519.934	3.059	1.25	7.25	1473.415	8	106.311
13b	520.922	8.245	1.25	8.75	1443.826	8	120.985
1	410.302	5.672	1	6.9	1210.677	6	63.336
2	380.535	1.98	0	4	1317.793	6	36.205
3	327.466	3.484	0	2.25	1184.963	6	18.947
4	339.439	4.647	1	3.5	1179.308	4	58.733
5	405.458	6.69	1	5.75	1277.266	1	91.621
6	406.486	2.674	1	6.25	1336.557	5	85.69
7	483.673	5.528	0	4.5	1601.507	2	36.533
9	407.419	7.867	0.25	7.95	1261.055	8	92.37

Table 7: Therapeutic significant parameters of all selected compounds

Com. Code	CNS	QPlogPo/w	QPlogS	QPPCaco	QPlogBB	QPPMDCK	metab	QPlogKhsa	Percent HOA
8	0	4.055	-4.966	3440.88	-0.157	4852.13	6	0.199	100
10	0	3.395	-4.523	1768.55	-0.458	2045.03	5	0.136	100
11a	-1	3.998	-5.498	1079.96	-0.717	1380.04	5	0.327	100
11b	0	5.429	-6.886	1719.52	-0.631	2081.97	5	0.753	100
11c	-2	4.645	-6.629	725.112	-1.155	622.903	6	0.55	100
11d	-2	4.124	-5.47	619.137	-1.034	730.372	7	0.303	100
11e	-2	4.533	-6.55	837.675	-1.018	1053.34	7	0.416	100
11f	-1	5.488	-7.708	1143.89	-0.9	1331.13	6	0.882	100
11g	0	5.832	-7.764	1482.68	-0.547	4358.63	6	0.905	91.933
11h	-1	5.799	-7.728	999.508	-0.706	3070.17	5	0.957	88.674
11i	0	6.238	-8.163	1438.08	-0.395	9138.64	5	1.02	94.07
11j	0	6.452	-8.771	1570.81	-0.36	10000	6	1.053	96.01
11k	-2	4.276	-7.821	192.833	-1.833	215.528	6	0.535	79.926
11l	-2	4.255	-6.14	548.897	-1.153	582.977	8	0.474	100
11m	-2	5.509	-7.67	960.689	-1.027	1116.05	7	0.908	73.708
11n	-1	4.299	-6.143	850.702	-0.92	1073.63	5	0.512	100
11o	-1	4.246	-5.45	933.394	-0.933	827.368	5	0.489	100
11p	0	5.243	-6.787	1887.32	-0.686	2528.77	5	0.721	100
11q	0	5.424	-6.344	2727.06	-0.377	3127.52	6	0.784	100
11r	0	5.405	-6.326	1625.90	-0.449	3734.57	6	0.764	90.146
11s	0	6.089	-6.975	2686.89	-0.114	10000	6	0.905	100
11t	-2	4.907	-7.629	694.959	-1.172	704.256	6	0.649	100
11u	-2	4.505	-6.625	665.601	-1.063	741.007	6	0.473	100
11v	0	4.521	-5.345	1600.13	-0.618	1593.24	7	0.415	100
12	0	4.046	-4.828	4028.93	-0.094	5303.92	5	0.195	100
13a	0	5.498	-7.088	1046.55	-0.659	2883.35	6	0.834	87.266
13b	-2	4.323	-6.614	390.529	-1.226	887.96	8	0.435	85.684
1	1	4.351	-5.577	4330.64	0.133	10000	4	0.291	100
2	1	5.91	-6.797	6493.50	0.004	3737.17	5	1.119	100
3	1	6.032	-6.504	9612.15	0.188	5710.35	6	1.201	100
4	0	5.052	-6.514	3919.05	-0.111	2165.25	4	0.978	100
5	0	4.389	-7.12	1034.58	-0.606	513.226	4	0.906	100
6	-1	4.56	-6.781	1379.43	-0.722	700.408	6	0.79	100
7	1	7.804	-10.225	6345.97	0.259	4817.53	6	1.979	100
9	-1	3.595	-6.035	1267.02	-0.666	2169.76	6	0.01	100

4. Conclusion

Depression, anxiety and post-traumatic stress disorders caused severe harmful effect on human beings. Due to the role of CRF in stress vulnerability and hyper-secretion in stress disorders, it makes an attractive target for anti-depressant drug development programme. In summary, we have obtained 2D and 3D-QSAR model using 27 substituted pyrazinone derivatives with different training sets. Both models were found to be robust, predictive and significant. In both models, a high r^2, q^2 and low standard value were found that indicated the robustness of the generated model. There were various 2D and 3D-descriptors calculated and their positive and negative contribution was evaluated. The results suggest that nitrogen substituted carbamate with an aromatic ring enhance the activity. Presence of the less bulky group and highly electronegative substituent at the R' position increases the antagonistic activity. The presence of sp^2 hybridized nitrogen, core heterocyclic ring involved the hydrophobic and hydrogen bond interaction with binding site. Docking results revealed that compound **11i** (2-(5-chloro-3-((6-methoxy-2,5-dimethylpyridin-3-yl)amino)-2-oxopyrazin-1(2*H*)-yl)-2-cyclopropylethyl (2,4-dichlorophenyl)carbamate) has binding affinity towards the binding pocket of target protein in comparison to all reference compounds. The residue of the CRF-1 protein involved in binding mechanism are Phe193, Tyr194, Trp119, Tyr139, Pro195, Tyr8, Trp287, Met19, Phe288, and Ala286 (hydrophobic), Asp284, Glu305 (hydrogen bonding) and Trp9 (π-π stacking). Simulation studies revealed that compound **11i** has better binding as compared to reference compound **2** (3-(6-(dimethylamino)-4-methylpyridin-3-yl)-2,5-dimethyl-*N*,*N*-dipropylpyrazolo[1,5-a]pyrimidin-7-amine). The presence of the NH group makes the compound lipophilic. Synthesized pyrazinone substituted compounds showed an excellent binding affinity and antagonistic activity as compared to reference compounds, thus design new antagonists of CRF-1 using observed information gained more potent and efficacious compounds. Relative binding energy and physicochemical parameters were also evaluated for all compounds. Most of the compounds including reference compounds shown excellent pharmacokinetic and therapeutic profile. Therefore, substituted pyrazinones could be potent and efficacious class for treatment of depression, anxiety and post-traumatic stress disorders.

Conflict of Interest

The authors declare that they have no competing interests.

Acknowledgements

The authors are thankful to Centre for Human Genetics & Molecular Medicine, Central University of Punjab for providing computational facilities to accomplish this research work.

References

Ahuja, V. T., Hartz, R. A., Molski, T. F., Mattson, G. K., Lentz, K. A., Grace, J. E., Macor, J. E. (2016). Synthesis and evaluation of carbamate and aryl ether substituted pyrazinones as corticotropin releasing factor-1 (CRF1) receptor antagonists. Bioorganic & Medicinal Chemistry Letters, 26(9), 2184–2187. doi:10.1016/j.bmcl.2016.03.067

Ajmani, S., Jadhav, K., & Kulkarni, S. A. (2006). Three-Dimensional QSAR Using the k-Nearest Neighbor Method and Its Interpretation. Journal of Chemical Information and Modeling, 46(1), 24–31. doi:10.1021/ci0501286

Desmond Molecular Dynamics System, D. E. Shaw Research, New York, NY, 2018. Maestro-Desmond Interoperability Tools, Schrödinger, New York, NY, 2018.

Dzierba, C. D., Hartz, R. A., & Bronson, J. J. (2008). Chapter 1 Recent Advances in Corticotropin-Releasing Factor Receptor Antagonists. Annual Reports in Medicinal Chemistry, 3–23. doi:10.1016/s0065-7743(08)00001-8

Friesner, R. A., Banks, J. L., Murphy, R. B., Halgren, T. A., Klicic, J. J., Mainz, D. T., Shenkin, P. S. (2004). Glide: A New Approach for Rapid, Accurate Docking and Scoring. 1. Method and Assessment of Docking Accuracy. Journal of Medicinal Chemistry, 47(7), 1739–1749. doi:10.1021/jm0306430

Gilligan, P. J., He, L., Clarke, T., Tivitmahaisoon, P., Lelas, S., Li, Y.-W., Trainor, G. (2009). 8-(4-Methoxyphenyl)pyrazolo[1,5-a]-1,3,5-triazines: Selective and Centrally Active Corticotropin-Releasing Factor Receptor-1 (CRF1) Antagonists. Journal of Medicinal Chemistry, 52(9), 3073–3083. doi:10.1021/jm9000242

Golbraikh A & Tropsha A, (2000) Predictive QSAR modeling based on diversity sampling of experimental datasets for the training and test set selection. Molecular diversity, 5(4); 231-243. doi:10.1023/a:1021372108686

Goyal, S., Dhanjal, J. K., Tyagi, C., Goyal, M., & Grover, A. (2014). Novel Fragment-Based QSAR Modeling and Combinatorial Design of Pyrazole-Derived CRK3 Inhibitors as Potent Antileishmanials. Chemical Biology & Drug Design, 84(1), 54–62. doi:10.1111/cbdd.12290

Grigoriadis, D., Haddach, M., Ling, N., & Saunders, J. (2001). The CRF Receptor Structure, Function and Potential for Therapeutic Intervention. Current Medicinal Chemistry-Central Nervous System Agents, 1(1), 63–97. doi:10.2174/1568015013358734

Hartz, R. A., Ahuja, V. T., Rafalski, M., Schmitz, W. D., Brenner, A. B., Denhart, D. J., Macor, J. E. (2009). In Vitro Intrinsic Clearance-Based Optimization ofN3-Phenylpyrazinones as Corticotropin-Releasing Factor-1 (CRF1) Receptor Antagonists. Journal of Medicinal Chemistry, 52(14), 4161–4172. doi:10.1021/jm900302q

Hartz, R. A., Ahuja, V. T., Schmitz, W. D., Molski, T. F., Mattson, G. K., Lodge, N. J., Macor, J. E. (2010). Synthesis and structure–activity relationships of N3-pyridylpyrazinones as corticotropin-releasing factor-1 (CRF1) receptor antagonists. Bioorganic & Medicinal Chemistry Letters, 20(6), 1890–1894. doi:10.1016/j.bmcl.2010.01.129

Hartz, R. A., Ahuja, V. T., Zhuo, X., Mattson, R. J., Denhart, D. J., Deskus, J. A., Bronson, J. J. (2009). A Strategy to Minimize Reactive Metabolite Formation: Discovery of (S)-4-(1-Cyclopropyl-2-methoxyethyl)-6-[6-(difluoromethoxy)-2,5-dimethylpyridin-3-ylamino]-5-oxo-4,5-dihydropyrazine-2-carbonitrile as a Potent, Orally Bioavailable Corticotropin-Releasing Factor-1 Receptor Antagonist†. Journal of Medicinal Chemistry, 52(23), 7653–7668. doi:10.1021/jm900716v

Hauger, R. L., Risbrough, V., Oakley, R. H., Olivares-Reyes, J. A., & Dautzenberg, F. M. (2009). Role of CRF Receptor Signaling in Stress Vulnerability, Anxiety, and Depression. Annals of the New York Academy of Sciences, 1179(1), 120–143. doi:10.1111/j.1749-6632.2009.05011.x

Kaur, P., Sharma, V., & Kumar, V. (2012). Pharmacophore Modelling and 3D-QSAR Studies on -Phenylpyrazinones as Corticotropin-Releasing Factor 1 Receptor Antagonists. International Journal of Medicinal Chemistry, 2012, 1–13. doi:10.1155/2012/452325

Kevin J. Bowers, Edmond Chow, Huafeng Xu, Ron O. Dror, Michael P. Eastwood, Brent A. Gregersen, John L. Klepeis, Istvan Kolossvary, Mark A. Moraes, Federico D. Sacerdoti, John K. Salmon, Yibing Shan, and David E. Shaw, Bowers, K. J., Chow, E., Xu, H., Dror, R. O.,

Eastwood, M. P., Gregersen, B. A., John, L., Klepeis, Kolossvary, I., Mark, A. M., Federico, D., Sacerdoti, J. K., Salmon, Yibing, S. & Shaw, D. E. (2006, November). Scalable algorithms for molecular dynamics simulations on commodity clusters. In SC 2006 Conference, Proceedings of the ACM/IEEE (pp. 43-43). IEEE. doi:10.1109/SC.2006.54

Kumar, H., Raj, U., Gupta, S., & Varadwaj, P. K. (2016). In-silico identification of inhibitors against mutated BCR-ABL protein of chronic myeloid leukemia: a virtual screening and molecular dynamics simulation study. Journal of Biomolecular Structure and Dynamics, 34(10), 2171–2183. doi:10.1080/07391102.2015.1110046

Kumar, N., Mishra, S. S., Sharma, C. S., Singh, H. P., & Kalra, S. (2017). In silico binding mechanism prediction of benzimidazole based corticotropin releasing factor-1 receptor antagonists by quantitative structure activity relationship, molecular docking and pharmacokinetic parameters calculation. Journal of Biomolecular Structure and Dynamics, 36(7), 1691–1712. doi:10.1080/07391102.2017.1332688

Li, J., Abel, R., Zhu, K., Cao, Y., Zhao, S., & Friesner, R. A. (2011). The VSGB 2.0 model: A next generation energy model for high resolution protein structure modeling. Proteins: Structure, Function, and Bioinformatics, 79(10), 2794–2812. doi:10.1002/prot.23106

Mochizuki, M., Kori, M., Kobayashi, K., Yano, T., Sako, Y., Tanaka, M., Aso, K. (2016). Design and Synthesis of Benzimidazoles As Novel Corticotropin-Releasing Factor 1 Receptor Antagonists. Journal of Medicinal Chemistry, 59(6), 2551–2566. doi:10.1021/acs.jmedchem.5b01715

Owens, m. J., & nemeroff, c. B. (1992). Stress, corticotropin-releasing factor neurons, and the actions of benzodiazepines. Clinical neuropharmacology, 15, 155a–156a. doi:10.1097/00002826-199201001-00083

Patil, R., Das, S., Stanley, A., Yadav, L., Sudhakar, A., & Varma, A. K. (2010). Optimized Hydrophobic Interactions and Hydrogen Bonding at the Target-Ligand Interface Leads the Pathways of Drug-Designing. PLoS ONE, 5(8), e12029. doi:10.1371/journal.pone.0012029

Pioszak, A. A., Parker, N. R., Suino-Powell, K., & Xu, H. E. (2008). Molecular Recognition of Corticotropin-releasing Factor by Its G-protein-coupled Receptor CRFR1. Journal of Biological Chemistry, 283(47), 32900–32912. doi:10.1074/jbc.m805749200

Sharma, C. S., Mishra, S., Singh, H., & Kumar, N. (2016). In silico ADME and Toxicity Study of Some Selected Antineoplastic Drugs. International Journal of Pharmaceutical Sciences and Drug Research, 8(01). doi:10.25004/ijpsdr.2016.080110

Shivakumar, D., Williams, J., Wu, Y., Damm,W., Shelley, J., Sherman, W., (2010) Prediction of Absolute Solvation Free Energies using Molecular Dynamics Free Energy Perturbation and the OPLS Force Field, J. Chem. Theory Comput. 6, 1509–1519. doi: 10.1021/ct900587b

Su, P.-C., & Johnson, M. E. (2015). Evaluating thermodynamic integration performance of the new amber molecular dynamics package and assess potential halogen bonds of enoyl-ACP reductase (FabI) benzimidazole inhibitors. Journal of Computational Chemistry, 37(9), 836–847. doi:10.1002/jcc.24274

Su, P.-C., Tsai, C.-C., Mehboob, S., Hevener, K. E., & Johnson, M. E. (2015). Comparison of radii sets, entropy, QM methods, and sampling on MM-PBSA, MM-GBSA, and QM/MM-GBSA ligand binding energies of F. tularensisenoyl-ACP reductase (FabI). Journal of Computational Chemistry, 36(25), 1859–1873. doi:10.1002/jcc.24011

Williams, J. P. (2013). Corticotropin-releasing factor 1 receptor antagonists: a patent review. Expert Opinion on Therapeutic Patents, 23(8), 1057–1068. doi:10.1517/13543776.2013.795545

Zorrilla, E. P., & Koob, G. F. (2004). The therapeutic potential of CRF1 antagonists for anxiety. Expert Opinion on Investigational Drugs, 13(7), 799–828. doi:10.1517/13543784.13.7.799